A bouncing ball model with two nonlinearities: a prototype for Fermi acceleration

2008 J. Phys. A: Math. Theor. 41 015104

(http://iopscience.iop.org/1751-8121/41/1/015104)

IOP PUBLISHING JOURNAL OF PHYSICS A: MATHEMATICAL AND THEORETICAL

J. Phys. A: Math. Theor. **41** (2008) 015104 (13pp) doi:10.1088/1751-8113/41/1/015104

A bouncing ball model with two nonlinearities: a prototype for Fermi acceleration

Edson D Leonel and Mario Roberto Silva

Departamento de Estatística, Matemática Aplicada e Computação, IGCE, Universidade Estadual Paulista, UNESP, Av. 24A, 1515, Bela Vista, 13.506-900 Rio Claro, SP, Brazil

Received 15 August 2007, in final form 31 October 2007
Published 12 December 2007
Online at stacks.iop.org/JPhysA/41/015104

Abstract

Some dynamical properties of a bouncing ball model under the presence of an external force modelled by two nonlinear terms are studied. The description of the model is made by the use of a two-dimensional nonlinear measure-preserving map on the variable's velocity of the particle and time. We show that raising the straight of a control parameter which controls one of the nonlinearities, the positive Lyapunov exponent decreases in the average and suffers abrupt changes. We also show that for a specific range of control parameters, the model exhibits the phenomenon of Fermi acceleration. The explanation of both behaviours is given in terms of the shape of the external force and due to a discontinuity of the moving wall's velocity.

PACS numbers: 05.45.−a, 05.45.Ac, 05.45.Pq

(Some figures in this article are in colour only in the electronic version)

1. Introduction

The bouncing ball model consists of a classical particle of mass m which is confined to bounce between two infinitely heavy and rigid walls [1]. One of the walls is assumed to be fixed while the other one moves in time according to a periodic function. This model, also known as the Fermi–Ulam model (FUM), is a simple dynamical system that can be modelled using the formalism of discrete mappings. Moreover, many tools developed to characterize such a model show to have a great applicability in more complex mappings. Considering the FUM, many results are known in the literature. Particularly for the particle suffering elastic collisions with either walls, it is known that the phase space of the model is of mixed kind [2] in the sense that depending on the combination of both the control parameters and initial conditions, invariant spanning curves limiting the size of chaotic seas and Kolmogorov–Arnold–Moser (KAM) islands can all be observed. The presence of the invariant spanning curves yields in a limit for the energy gain of a bouncing particle, thus the Fermi acceleration (unlimited energy gain of the particle) is not observed. A similar version of the model, called as bouncer [3], consists of

a classical particle, in the presence of a constant gravitational field, suffering elastic collisions with a periodically moving platform. The returning mechanism of the bouncer model, a mechanism that injects the particle for a next collision with the moving wall, is rather distinct from the FUM. In the bouncer, it is due only to the gravitational field while in the FUM it is given by a collision with a fixed wall. These differences yield in a profound consequence for the dynamics of a bouncing particle. Depending on the control parameter, the unlimited energy gain is observed in the bouncer model, a phenomenon that is not present in the FUM with periodic and smooth oscillations. The differences were clarified by Lichtenberg *et al* [4]. Hybrid versions of the FUM and bouncer were recently studied [5, 6], as well as a stochastic version of the FUM [7].

There are also many important results concerning the inclusion of damping forces on both the models (see, for example [8] for a short review). One of them is the presence of a drag force [9], so that the particle is moving inside a gas with the dissipation acting on the particle along its trajectory. The dynamics of the problem is, generally, given by a nonlinear mapping that is obtained via the solution of Newton's law. A different kind of dissipation can be introduced via inelastic hits of the particle with the walls. Thus, there is a restitution coefficient that makes the particle experiences a fractional loss of energy upon collisions. Despite both kinds of damping often occur in nature, they have profound and different consequences in the dynamics of the models. As an example, in [10, 11] and considering inelastic collisions, Tsang and Lieberman considered the simplified FUM (both the walls are fixed but the particle changes energy and momentum upon collisions with one of the walls as if the wall were moving) with inelastic impacts. They have evidenced contraction on the phase space and, in particular, observed the presence of a strange attractor. Recently, a rather similar version of the dissipative model [12] confirmed the property of area contraction and, in addition, a boundary crisis was characterized. Additionally, a family of boundary crisis was observed when collisions with the two walls are inelastic [13]. The bouncer model was also considered under inelastic collisions. For example, in [14] Holmes discusses the appearances of horseshoes in the inelastic bouncer and gave an illustration of a homoclinic orbit in such a model. After that, Everson [15] presents and discusses with many numerical simulations the appearance of period doubling cascade in the damping bouncer model. Period doubling cascade was also observed in [16] for the completely inelastic collisions. The presence of frictional force however was considered by Luna-Acosta [17] and Naylor *et al* [18] in the bouncer model. They too observed period doubling cascades and in special Luna-Acosta [17] has achieved analytically dimensional reduction for the limit of high dissipation.

In this paper, we study a non-dissipative version of a bouncing ball model seeking to understand and describe some of its dynamical properties considering however that the motion of the moving wall is given via a crank-connecting rod scheme. For such a scheme, it is known that there are two nonlinearities present in the model and each of them play important rules in the dynamics. Depending on certain ranges of control parameters, there can be profound consequences on the dynamics of the system. Particularly, when one of the two control parameters is raised, the positive Lyapunov exponent experiences a drastic reduction. It is also important to say that the particle is in the total absence of any external field. Other important result for this model is that it yields, for specific control parameter values, the phenomenon of Fermi acceleration (unlimited energy growth). The phenomenon is characterized, for the first time in the present model, in terms of a discontinuity of the derivative of the wall's position with respect to the time, thus leading the particle to acquire unlimited energy gain.

This paper is organized as follows. In section 2, we present the model and the expressions of the mapping that fully describes the dynamics of the system. Section 2 is also devoted to a

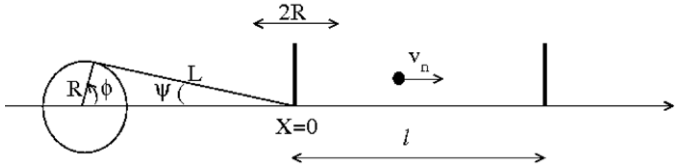

Figure 1. Illustration of the model under consideration.

discussion of the numerical results and the behaviour of the positive Lyapunov exponent. In section 3, we propose a simplified version of the model and study the behaviour of the average velocity as a function of a control parameter. We show that the Fermi acceleration emerges naturally from the deterministic dynamics of the model for specific control parameter values. Final remarks and conclusions are drawn in section 4.

2. The model and the mapping

The model is described using a two-dimensional mapping for the variables (v_n, t_n), where v_n and t_n are the corresponding velocity of the particle and time immediately after the nth collision with the moving wall. We assume that one wall is fixed at $x = l$ and that the motion of the moving wall is given by $s(t) = R\cos(wt) + \sqrt{L^2 - R^2\sin^2(wt)}$ (we stress the term wt in the equation of $s(t)$ is represented by the variable ϕ in figure 1), where R denotes the radii of the crank, L the length of the connecting rod and w the corresponding frequency of oscillation. Figure 1 illustrates the model under consideration. We stress the equation for $s(t)$ is easily obtained from the condition of $R\sin(\phi) = L\sin(\psi)$, as can be seen in figure 1. Before we write the equations of the mapping, let us first discuss the initial conditions. We assume that, at a time $t = t_n$, the particle is at the position $x_p(t_n) = s(t_n)$ with velocity $v = v_n > 0$. Thus, such an initial condition can be considered as if the dynamics were already running in the system along the time. We emphasize that two different kinds of collisions can be observed, namely, (i) multiple hits with the moving wall and (ii) a single hit with the moving wall. In case (i), the particle suffers a collision with the moving wall but then, before it leaves the collision zone, which is defined as $x \in [-R, R]$, the particle experiences a second and then successive impact with the moving wall. Such kind of collisions becomes rare in the limit of high energy but they are quite often to be observed in the regime of low energy. It is also easy to see that there are too many control parameters in the model, four in total, namely, R, L, l and w, and that the dynamics of the system does not depend on all of them. It is convenient to define dimensionless and more appropriate variables. We define $\epsilon = R/l, r = R/L, V_n = v_n/(wl)$ and measure the time in terms of the number of oscillations of the moving wall $\phi_n = wt_n$. For the dimensionless variables, we consider that the range for ϵ is $\epsilon \in [0, 1]$ and for r is $r \in [0, 1]$. The limit of $r \to 0$ corresponds to $L \to \infty$ and $r \to 1$ is obtained for $L \to R^+$. With this new set of variables, the mapping that describes the dynamics of the system is written as

$$T : \begin{cases} \phi_{n+1} = [\phi_n + \Delta T_n] \bmod(2\pi) \\ V_{n+1} = V_n^* - 2\epsilon\sin(\phi_{n+1})\left[1 + \dfrac{r\cos(\phi_{n+1})}{\sqrt{1 - r^2\sin^2(\phi_{n+1})}}\right], \end{cases} \tag{1}$$

where the expressions of V_n^* and ΔT_n depend on the kind of collision. For case (i), which corresponds to the multiple hits with the moving wall, the corresponding expressions are

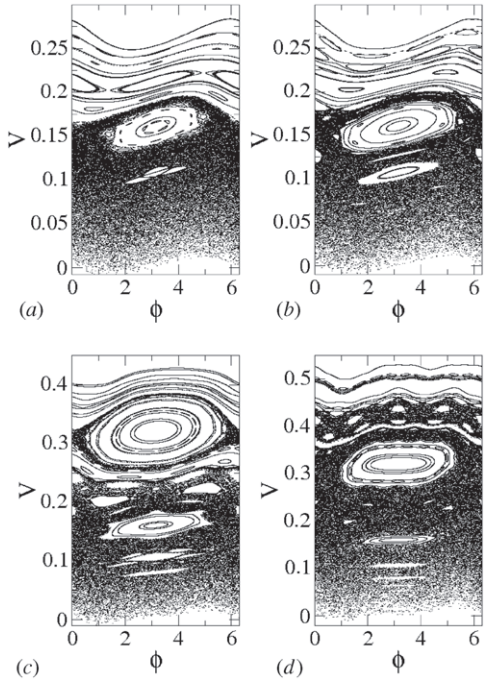

Figure 2. Phase space generated from the mapping (1) and control parameters $\epsilon = 0.01$ and (*a*) $r = 0.1$, (*b*) $r = 0.3$, (*c*) $r = 0.6$ and (*d*) $r = 0.9$.

$V_n^* = -V_n$ and $\Delta T_n = \phi_c$ with ϕ_c obtained by the solution of $G(\phi_c) = 0$ with $G(\phi_c)$ given by

$$G(\phi_c) = \epsilon\cos(\phi_n + \phi_c) - \epsilon\cos(\phi_n) - V_n\phi_c + \frac{\epsilon}{r}\sqrt{1 - r^2\sin^2(\phi_n + \phi_c)} - \frac{\epsilon}{r}\sqrt{1 - r^2\sin^2(\phi_n)}. \tag{2}$$

A solution of the function $G(\phi_c)$ for $\phi_c \in (0, 2\pi]$ corresponds to a collision of the particle with the moving wall and is obtained numerically.

Let us now consider the case where the particle leaves the collision zone, i.e. case (ii). The corresponding expressions are $V_n^* = V_n$, $\Delta T_n = \phi_T + \phi_c$, where ϕ_T corresponds to the elapsed time the particle spends travelling from the last hit with the moving wall, up to suffering an elastic reflection with the static wall and be reflected backwards, therefore until the entrance of the moving wall. Thus, ϕ_T is given by

$$\phi_T = \frac{2 + \left(\frac{\epsilon}{r} - \frac{\epsilon}{r}\sqrt{1 - r^2\sin^2(\phi_n)}\right) - \epsilon\cos(\phi_n) - \epsilon}{V_n}. \tag{3}$$

The term ϕ_c is numerically obtained from $F(\phi_c) = 0$ for $\phi_c \in [0, 2\pi)$, where the function $F(\phi_c)$ is given by

$$F(\phi_c) = \epsilon\cos(\phi_n + \phi_T + \phi_c) + \frac{\epsilon}{r}\sqrt{1 - r^2\sin^2(\phi_n + \phi_T + \phi_c)} - \frac{\epsilon}{r} - \epsilon + V_n\phi_c. \tag{4}$$

After some straightforward algebra, it is easy to show that the mapping (1) preserves the following phase space measure:

$$\mathrm{d}\mu = \left[V + \epsilon\sin(\phi)\left(1 + \frac{r\cos(\phi)}{\sqrt{1 - r^2\sin^2(\phi)}}\right)\right]\mathrm{d}V\,\mathrm{d}\phi. \tag{5}$$

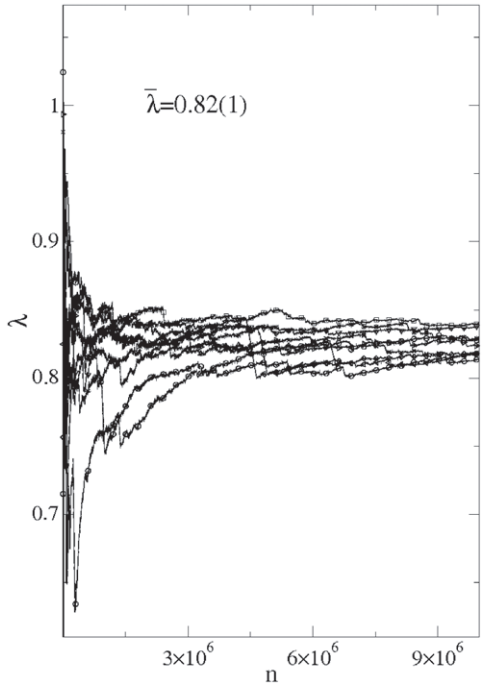

Figure 3. Positive Lyapunov exponent for ten different initial conditions randomly chosen along the chaotic sea in the low-energy regime. The control parameters used were $\epsilon = 0.01$ and $r = 0.1$.

We stress that in the limit of $r \to 0$, the results for the one-dimensional Fermi accelerator model are all recovered [5, 19].

Figure 2 shows the corresponding phase space obtained via the iteration of the mapping (1) for the control parameters $\epsilon = 0.01$ and (*a*) $r = 0.1$, (*b*) $r = 0.3$, (*c*) $r = 0.6$ and (*d*) $r = 0.9$. We can clearly see that the shape of the phase space changes as the control parameter r varies. On the other hand, the mixed form is preserved in the sense that a large chaotic sea, which surrounds KAM islands, is limited by a set of invariant spanning curves. One can also note that the position of the lowest invariant spanning curve raises as the control parameter r increases. In our simulations, we will consider the values for r that may approach the unity, moreover in the range of $r \in [0, 1]$. However for a real experimental system, in which damping forces cannot be neglected, such values for r have no much interest. This is mainly because the damping force can acquire larger values as compared to the component of the force with respect to the motion (for instance, it happens for large values of the angle ψ) and therefore lead the system to reach the rest.

The two natural questions that we are interested in concern on the properties of the chaotic sea (see figure 2), are the positive Lyapunov exponent and the average velocity of the particle. Our main goal is to describe their behaviour as a function of the control parameter r. We think this study is of interest because the control parameter r directly controls the straight of a nonlinearity of the model. For small values of r, results of the FUM should be obtained. Moreover, we expect that the results obtained for $r \to 1$ contribute towards a better understanding of this model for such a range of r and, in particular, as we will see in section 3, in a description of the phenomenon of Fermi acceleration. The behaviour of the Lyapunov exponent is described in this section while the average velocity is discussed in section 3.

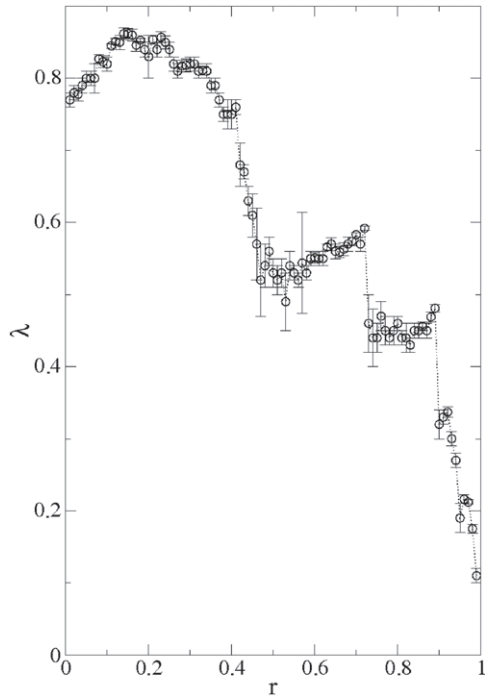

Figure 4. Positive Lyapunov exponent as a function of r for a fixed $\epsilon = 0.01$.

We concentrate to investigate the behaviour of the positive Lyapunov exponent for the chaotic sea. It is well known that the Lyapunov exponent is commonly used as a tool to characterize the sensitivity to initial conditions. Figure 3 shows the asymptotic convergence of the positive Lyapunov exponent for the control parameters $\epsilon = 0.01$ and $r = 0.1$. The ensemble average of ten different initial conditions randomly chosen along the chaotic sea gives $\bar{\lambda} = 0.82 \pm 0.01$, where the error 0.01 denotes the standard deviation of the ten samples. Each initial condition was iterated up to 10^7 collisions with the moving wall. The method used to obtain the Lyapunov exponents is described in the appendix.

Let us discuss the behaviour of the positive Lyapunov exponent as a function of r. Figure 4 shows the behaviour of $\lambda \times r$. We can see that, in the limit of $r \to 0$, the positive Lyapunov exponent recovers the value of the one-dimensional Fermi accelerator model [5, 19]. The positive Lyapunov exponent then grows slightly, having a maximum value around $r = 0.15$ and then decreases almost monotonically until around $r = 0.5$. Then it starts growing again until $r \approx 0.7$ when it suddenly decreases. Other abrupt change is observed for $r \approx 0.89$. Thus, the two main questions that arise from figure 4 are (i) why does the positive Lyapunov exponent decreases in the average, instead of growth, as r raises? (ii) what is the explanation of the abrupt changes in λ?

The answer for question (i) comes from the shape of the function that describes the motion of the moving wall. Figure 5 shows four different plots of $S(\phi) = r\cos(\phi) + \sqrt{1 - r^2\sin^2(\phi)}$ (for the sake of clarity, we show two periods in ϕ for $S(\phi)$), which describes the motion of the moving wall for four different values of r, namely, (a) $r = 0.1$, (b) $r = 0.4$, (c) $r = 0.8$ and (d) $r = 0.999$. For $r = 0.1$ the function looks like a cosine function, but as r increases the shape changes substantially. It thus become to have two regimes of variation where one of

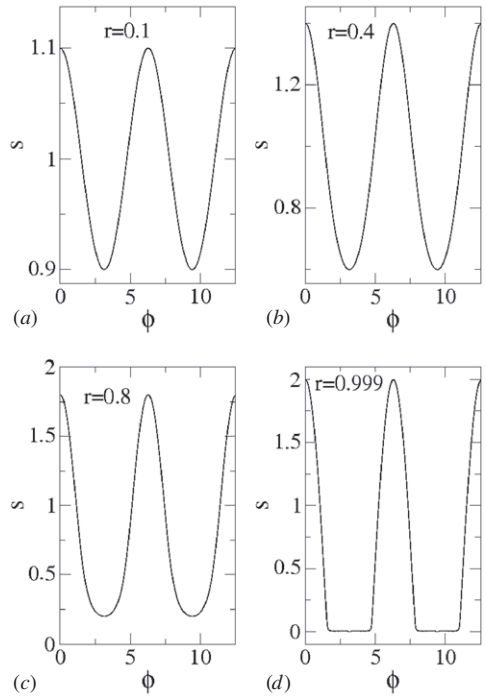

Figure 5. Plot of $S(\phi)$ for two periods in ϕ considering the control parameters $\epsilon = 0.01$ and (*a*) $r = 0.1$, (*b*) $r = 0.4$, (*c*) $r = 0.8$ and (*d*) $r = 0.999$.

them is characterized by a constant plateau in the limit of $r \to 1$, as can be seen in the range of $\phi \in (\pi/2, 3\pi/2)$ and a regime of fast variation, which is given by the complementary values of ϕ. In the limit case of $r = 1$, the function $S(\phi)$ has indeed discontinuities in its derivative for two values of ϕ, namely, $\phi = \pi/2$ and $\phi = 3\pi/2$. As we will see in the following section, the discontinuities for $\dot{S}(\phi)$ yield a profound consequence in the dynamics of the system thus leading the particle to exhibit unlimited energy growth. The large plateaus imply that the particle, when suffers collisions with the moving wall, does not change substantially its velocity value since such plateaus lead in an 'almost' null velocity for the moving wall. Thus, the time that the particle spends until the next hit with the moving wall is almost the same as it spent in the previous collisions. It then implies that the particle, in a chaotic orbit, can experience many more collisions with the moving wall without substantially changing its energy as it would experiences if the plateaus were absent. Then, the form of $S(\phi)$ for large values of r yields in reducing the chaoticity of the system in the average.

We will now discuss a possible answer for question (ii), i.e. the explanation of the sudden changes in λ. They are basically related to the destruction of the lowest energy invariant spanning curve together with a destruction of small chaotic layers. Considering the case of low energy and for $r = 0.69$, the system has a large chaotic sea (the black region of figure 6(*c*)) which shares boundary with a thin chaotic layer (the red region of figure 6(*c*)), as can be seen in figure 6. Above this chaotic layer, there is an invariant spanning curve (brown curve of figure 6(*c*)). Above yet of such curve we can see two thin chaotic layers (light blue and dark blue) and a relatively large chaotic sea (green region) surrounding a KAM island (see, for instance, figure 2(*c*)). Each of these chaotic regions were characterized in terms of Lyapunov exponents. Their corresponding values were: for the black region we obtained $\lambda_b = 0.574(6)$,

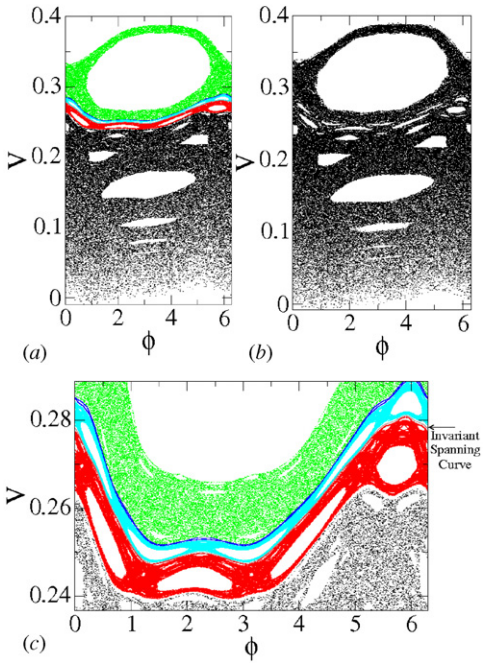

Figure 6. (*a*) Illustration of the chaotic behaviour generated by five different initial conditions for the control parameters $\epsilon = 0.01$ and $r = 0.69$. (*b*) Iteration of a single initial condition, evidencing the chaotic behaviour, for $\epsilon = 0.01$ and $r = 0.72$. (*c*) Zoom in of part (*a*) where it is easy to see an invariant spanning curve and chaotic layers.

for the red region $\lambda_r = 0.072(1)$, for the light blue region $\lambda_{lb} = 0.0110(4)$, for the dark blue region $\lambda_{db} = 0.0152(2)$ and for the green region $\lambda_g = 0.218(1)$. For $r = 0.72$, which is quite close to $r = 0.69$, those regions shown in figure 6(*a*) were all merged into a single and large chaotic sea characterized by a positive Lyapunov exponent $\lambda = 0.46(5)$. The merged regions are shown in figure 6(*b*). After the destruction of the thin structures shown in figure 6(*a*), the chaotic sea in the low-energy region can spreads over a larger accessible region of the phase space. So we can consider that, after the transition, the positive Lyapunov exponent could be obtained by an average of the previous values for the corresponding chaotic regions therefore taking into account the fraction of area occupied individually by each region. To check whether this supposition is correct, we have obtained the fraction of each chaotic region previous to the control parameter variation, i.e. for $r = 0.69$. We have defined a grid of 84 initial conditions for the ϕ-axis, limited to the interval $\phi \in [0, 2\pi)$, and 127 for the V-axis considering the interval $V \in [0, 0.38813]$. The value 0.38813 corresponds to the higher value of the velocity obtained for the chaotic sea shown in the green region of figure 6(*c*). Thus, in the total, we considered 10 668 different initial conditions. Each of them were evolved in time for $n = 10^7$ collisions with the moving wall and their Lyapunov exponents evaluated. The obtained value was compared to the Lyapunov exponent of the chaotic regions so that we were able to compare the corresponding fraction of initial conditions which belongs to one region or to another one. Applying this procedure for all the chaotic regions shown in figure 6(*c*), we found that the black chaotic sea fills a fraction of $P_b = 0.8261$ of the entire chaotic region. The red region corresponds to $P_r = 0.0279$, when the light blue region has a fraction of $P_{lb} = 0.0103$, the dark blue region is $P_{db} = 0.0038$ and finally the green region corresponds

to a fraction of $P_g = 0.1319$. After the transition, we could assume that the positive Lyapunov exponent is obtained by

$$\bar{\lambda} = \lambda_b P_b + \lambda_r P_r + \lambda_{lb} P_{lb} + \lambda_{db} P_{db} + \lambda_g P_g. \tag{6}$$

Evaluating equation (6) we found $\bar{\lambda} = 0.50$ which is a rather acceptable value as compared to the value obtained via numerical simulation of the chaotic sea after the destruction $\lambda = 0.46(5)$.

The abrupt change in λ around the value of $r \approx 0.89$ is explained by using the same arguments. We stress that similar results were observed in a rather distinct model [20].

3. A simplified version of the model and Fermi acceleration

Other important conclusion that arises from the shape of the function $S(\phi)$ is related to the energy gain of the bouncing particle. As r approaches the unity, the variation of the moving wall position becomes faster for specific ranges of ϕ. It implies that the particle can acquire, for specific ranges of ϕ, large values of velocity upon collisions with the moving wall for those regions of fast variation of $S(\phi)$. Such a result can be seen in figure 2 by the position of the lowest energy invariant spanning curve which assume higher values as the control parameter r raises. To illustrate such an argument more clearly, it is important to look at the behaviour of the average velocity for a sufficiently long time. To do this, we will make use of a simplification in the mapping (1) with the main goal of speeding up our numerical simulations and avoid solving the equations $G(\phi_c) = 0$ and $F(\phi_c) = 0$. This simplification, which is commonly used in the literature (see [1, 5, 7, 21–23]), consists in assuming that both walls are fixed. However, when the particle hits one of them, it exchanges energy and momentum as if the wall were moving. This procedure retains the nonlinearity of the problem and yields a huge advantage of avoid solving transcendental equations. The mapping is then given by

$$T : \begin{cases} \phi_{n+1} = \left[\phi_n + \dfrac{2}{V_n}\right] \bmod(2\pi) \\ V_{n+1} = \left| V_n - 2\epsilon \sin(\phi_{n+1}) \left[1 + \dfrac{r\cos(\phi_{n+1})}{\sqrt{1 - r^2 \sin^2(\phi_{n+1})}}\right]\right|. \end{cases} \tag{7}$$

Although this simplification brings the advantage of allowing very fast simulations as compared to those of the complete version, it also gives rise to a problem that we need to avoid. In the complete model, depending on the combination of both the velocity and phase of the moving wall, it is possible for the particle, after suffering a collision with the time-varying wall, to suffer a second successive collision before exiting the collision area, as well as possibly having a negative velocity following the first such collision. In the simplified model, non-positive velocities are forbidden because they are equivalent to the particle travelling beyond the wall. In order to avoid such problems, if after the collision the particle has a negative velocity, we inject it back with the same modulus of velocity. Such a procedure is effected perfectly by the use of a modulus function. Note that the velocity of the particle is reversed by the modulus function only if, after the collision, the particle remains travelling in the negative direction. The modulus function has no effect on the motion of the particle if it moves in the positive direction after the collision. We stress that this approximation is valid only for small values of ϵ.

We now discuss the procedure used to obtain the average velocity of the particle. First, we obtain the average velocity proceeding with an average over the orbit, i.e.

$$V_i = \frac{1}{n} \sum_{j=1}^{n} V_{i,j}, \tag{8}$$

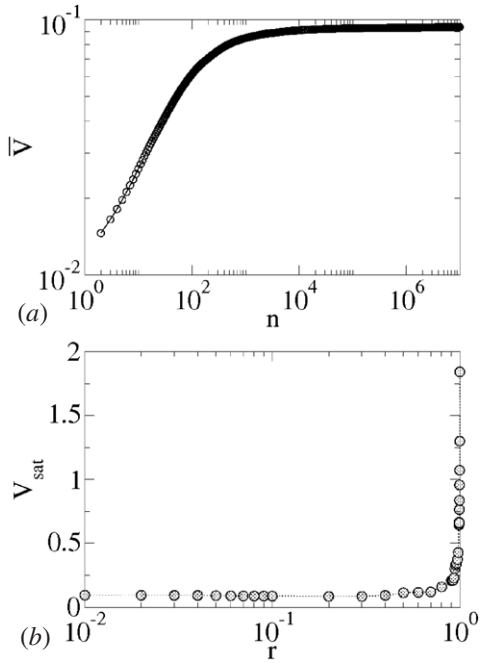

Figure 7. (*a*) Behaviour of $\bar{V} \times n$ for the control parameters $r = 0.01$ and $\epsilon = 0.01$. (*b*) Plot of $V_{\text{sat}} \times r$ for a fixed $\epsilon = 0.01$.

where j denotes the number of collisions. The second average is made in an ensemble of $M = 10^3$ different initial conditions so that the average value is defined as

$$\bar{V} = \frac{1}{M} \sum_{i=1}^{M} V_i, \tag{9}$$

with i corresponding to a sample in an ensemble of M different initial conditions.

Figure 7(*a*) shows the behaviour of $\bar{V} \times n$ for the control parameters $\epsilon = 0.01$ and $r = 0.01$ considering $n = 10^7$ iterations. We can see that the velocity of the particle grows for short iterations and then suddenly bends towards a regime of saturation for sufficiently long time. Moreover, we are interested in the behaviour of the asymptotic values of $\bar{V}$. Figure 7(*b*) shows the behaviour of $\bar{V}$ for long iterations, which we will refer to as V_{sat}. The behaviour of V_{sat} can be described for two different ranges of r. The first range is for $r < 0.9$ where we can see that V_{sat} is almost constant for the region of $r \in [0, 0.9)$. The second range of r is considered for $r \geqslant 0.9$. It is important to say that, when $r = 1$, the expression of the 'moving wall' velocity presents discontinuities for $\phi = \pi/2$ and $\phi = 3\pi/2$. Thus, it is convenient to define a new parameter $\mu = 1 - r$ and then study the behaviour of V_{sat} as a function of μ. This new control parameter has a practical application because it brings the criticality of the model to $\mu = 0$. Figure 8 shows the behaviour of $V_{\text{sat}} \times \mu$ for a fixed control parameter $\epsilon = 0.01$. We can describe such a behaviour according to

$$V_{\text{sat}} \propto \mu^{\alpha}. \tag{10}$$

After fitting a power law in figure 8, we obtain $\alpha = -0.460(6) \cong -0.5$. This kind of behaviour for V_{sat} confirms that, in the limit of $r \to 1$, the present model shows the phenomenon of Fermi acceleration. This result has a clear explanation in terms of the KAM theorem. As

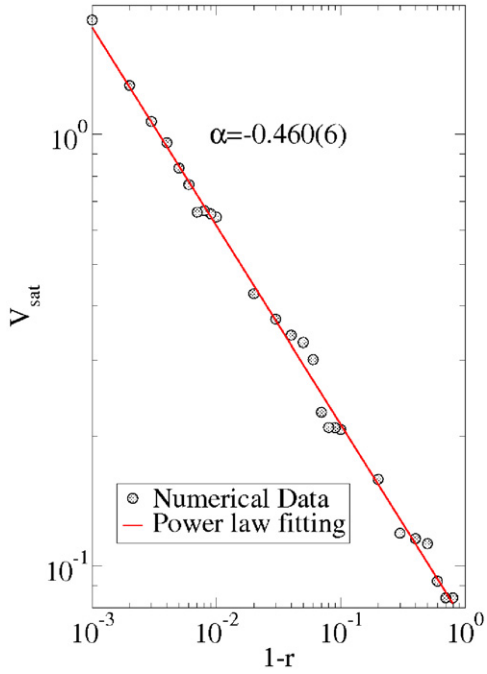

Figure 8. Plot of $V_{\text{sat}} \times \mu$ for a fixed $\epsilon = 0.01$. A power-law fitting gives that $\alpha = -0.460(6) \cong -0.5$.

was discussed by Lichtenberg *et al* [4], if the expression of the periodic wall's velocity has a sufficient number of continuous derivatives, then it is possible to obtain invariant spanning curves separating different portions of the phase space. Particularly, they are useful to prevent unlimited energy growth for a bouncing particle. Moreover, it was estimated by Moser [24] that three continuous derivatives for the moving wall's velocity is a sufficient condition for the existence of KAM surfaces (for instance, invariant spanning curves). However, in the present model and considering the limit of $r \to 1$, the expression of the velocity shows discontinuities for $\phi = \pi/2$ and $\phi = 3\pi/2$, so that the invariant spanning curves are not observed for $r = 1$ and consequently, the Fermi acceleration is present.

4. Conclusions

In summary, we have studied a non-dissipative version of a classical bouncing ball model under the presence of two nonlinearities. Our results show that, as one of the two control parameters varies, the positive Lyapunov exponent diminish in the average and experiences sudden changes. We have explained such a behaviour by the shape of the moving wall and due to the destruction of invariant spanning curves and thin chaotic layers. We have also shown that in the limit of $r \to 1$, the present model exhibits unlimited energy growth. This phenomenon was explained by using a discontinuity of the moving wall's velocity.

Acknowledgments

EDL thanks Professor Tadashi Yokoyama for fruitful discussions. Support from CNPq, FAPESP and FUNDUNESP, Brazilian agencies is gratefully acknowledged.

Appendix

In this appendix, we briefly discuss the procedure used to obtain the Lyapunov exponents. In effect, the procedure consists in evolving the system over a long time from two slightly different initial conditions. If the two trajectories diverge exponentially in time the orbit is called chaotic, and the Lyapunov exponent obtained is positive. If the Lyapunov exponent is negative, the orbit may be either periodic or quasi-periodic. Let us now describe the procedure used to obtain the Lyapunov exponents numerically. They are defined as [25]

$$\lambda_j = \lim_{n\to\infty} \ln|\Lambda_j|, \qquad j = 1, 2,$$

where Λ_j are the eigenvalues of $M = \prod_{k=1}^{n} J_k(V_k, \phi_k)$ and J_k is the Jacobian matrix evaluated over the orbit (V_k, ϕ_k). The Jacobian matrix is defined as

$$J = \begin{pmatrix} \frac{\partial V_{n+1}}{\partial V_n} & \frac{\partial V_{n+1}}{\partial \phi_n} \\ \frac{\partial \phi_{n+1}}{\partial V_n} & \frac{\partial \phi_{n+1}}{\partial \phi_n} \end{pmatrix}.$$

In order to evaluate the eigenvalues of M, we use the fact that J can be written as a product of $J = \Theta T$, where Θ is an orthogonal matrix and T is a right upper triangular one. We now define the elements of these matrices as

$$\Theta = \begin{pmatrix} \cos(\theta) & -\sin(\theta) \\ \sin(\theta) & \cos(\theta) \end{pmatrix}, \qquad T = \begin{pmatrix} T_{11} & T_{12} \\ 0 & T_{22} \end{pmatrix}.$$

Since M is defined as $M = J_n J_{n-1} \cdots J_2 J_1$, we can introduce the identity operator, rewrite M as $M = J_n J_{n-1} \cdots J_2 \Theta_1 \Theta_1^{-1} J_1$, and define $\Theta_1^{-1} J_1 = T_1$. The product $J_2 \Theta_1$ defines a new matrix J_2^*. In the following step, we may write M as $M = J_n J_{n-1} \cdots J_3 \Theta_2 \Theta_2^{-1} J_2^* T_1$. The same procedure yields $T_2 = \Theta_2^{-1} J_2^*$. The problem is thus reduced to the evaluation of the diagonal elements of $T_i : T_{11}^i, T_{22}^i$. Using the Θ and T matrices, we find the eigenvalues of M, given by

$$T_{11} = \frac{j_{11}^2 + j_{21}^2}{\sqrt{j_{11}^2 + j_{21}^2}}, \qquad T_{22} = \frac{j_{11} j_{22} - j_{12} j_{21}}{\sqrt{j_{11}^2 + j_{21}^2}}.$$

We can then evaluate the Lyapunov exponent using the relation

$$\lambda_j = \lim_{n\to\infty} \sum_{k=1}^{n} \frac{1}{n} \ln |T_{jj}^k|, \qquad j = 1, 2.$$

It is interesting to observe that $\lambda_1 = -\lambda_2$, because the map is measure preserving.

References

[1] Lichtenberg A J and Lieberman M A 1992 *Regular and Chaotic Dynamics, Applied Mathematical Sciences* vol 38 (New York: Springer)

[2] Lieberman M A and Lichtenberg A J 1972 *Phys. Rev.* A **5** 1852

[3] Pustylnikov L D 1977 *Tr. Moskov. Mat. Obsc.* **34** 1

[4] Lichtenberg A J, Lieberman M A and Cohen R H 1980 *Physica* D **1** 291

[5] Leonel E D and McClintock P V E 2005 *J. Phys. A: Math. Gen.* **38** 823

[6] Ladeira D G and Leonel E D 2007 *Chaos* **17** 023229

[7] Karlis A K, Papachristou P K, Diakonos F K, Constantoudis V and Schmelcher P 2006 *Phys. Rev. Lett.* **97** 194102
Karlis A K, Papachristou P K, Diakonos F K, Constantoudis V and Schmelcher P 2007 *Phys. Rev.* E **76** 016214

[8] Leonel E D and McClintock P V E 2006 *J. Phys. A: Math. Gen.* **39** 11399

[9] Leonel E D and McClintock P V E 2006 *Phys. Rev.* E **73** 066223

[10] Tsang K Y and Lieberman M A 1986 *Physica* D **21** 401
[11] Lieberman M A and Tsang K Y 1985 *Phys. Rev. Lett.* **5** 908
[12] Leonel E D and McClintock P V E 2005 *J. Phys. A: Math. Gen.* **38** L425
[13] Leonel E D and Egydio de Carvalho R 2007 *Phys. Lett.* A **364** 475
[14] Holmes P J 1982 *J. Sound Vib.* **84** 173
[15] Everson R M 1986 *Physica* D **19** 355
[16] Luck J M and Mehta A 1993 *Phys. Rev.* E **48** 3988
[17] Luna-Acosta G A 1990 *Phys. Rev.* A **42** 7155
[18] Naylor M A, Sánchez P and Swift M R 2002 *Phys. Rev.* E **66** 57201
[19] Leonel E D, da Silva J K L and Kamphorst S O 2004 *Physica* A **331** 435
[20] Leonel E D and da Silva J K L 2003 *Physica* A **323** 181
[21] Leonel E D, McClintock P V E and da Silva J K L 2004 *Phys. Rev. Lett.* **93** 014101
[22] Ladeira D G and da Silva J K L 2006 *Phys. Rev.* E **73** 026201
[23] da Silva J K L, Ladeira D G, Leonel E D, McClintock P V E and Kamphorst S O 2006 *Braz. J. Phys.* **36** 700
[24] Moser J 1973 *Stable and Random Motions in Dynamical Systems* (*Annals of Mathematical Studies* vol 77*)* (Princeton, NJ: Princeton University Press)
[25] Eckmann J P and Ruelle D 1985 *Rev. Mod. Phys.* **57** 617